Astronomy & Astrophysics manuscript no. crab_paper
January 19, 2018

Crab nebula polarization observations at 150 GHz with NIKA

A. Ritacco[1,8⋆], J.F. Macías-Pérez[1], N. Ponthieu[10], R. Adam[1,2], P. Ade[5], P. André[4], A. Beelen[6], A. Benoît[7], A. Bideaud[7], N. Billot[8], O. Bourrion[1], A. Bracco[4], M. Calvo[7], A. Catalano[1], G. Coiffard[3], B. Comis[1], A. D'Addabbo[7,9], F.-X. Désert[10], S. Doyle[5], J. Goupy[7], C. Kramer[8], G. Lagache[11], S. Leclercq[3], J.-F. Lestrade[17], P. Mauskopf[5,12], F. Mayet[1], A. Maury[4], A. Monfardini[7], F. Pajot[6], E. Pascale[5], L. Perotto[1], G. Pisano[5], M. Rebolo-Iglesias[1], V. Revéret[4], L. Rodriguez[4], C. Romero[3], H. Roussel[16], F. Ruppin[1], K. Schuster[3], A. Sievers[8], C. Thum[8], S. Triqueneaux[7], C. Tucker[5], and R. Zylka[3]

[1] Laboratoire de Physique Subatomique et de Cosmologie, Université Grenoble Alpes, CNRS/IN2P3, 53, avenue des Martyrs, Grenoble, France
[2] Laboratoire Lagrange, Université Côte d'Azur, Observatoire de la Côte d'Azur, CNRS, Blvd de l'Observatoire, CS 34229, 06304 Nice cedex 4, France
[3] Institut de RadioAstronomie Millimétrique (IRAM), Grenoble, France
[4] Laboratoire AIM, CEA/IRFU, CNRS/INSU, Université Paris Diderot, CEA-Saclay, 91191 Gif-Sur-Yvette, France
[5] Astronomy Instrumentation Group, University of Cardiff, UK
[6] Institut d'Astrophysique Spatiale (IAS), CNRS and Université Paris Sud, Orsay, France
[7] Institut Néel, CNRS and Université Grenoble Alpes, France
[8] Institut de RadioAstronomie Millimétrique (IRAM), Granada, Spain
[9] Dipartimento di Fisica, Sapienza Università di Roma, Piazzale Aldo Moro 5, I-00185 Roma, Italy
[10] Univ. Grenoble Alpes, CNRS, IPAG, F-38000 Grenoble, France
[11] Aix Marseille Université, CNRS, LAM (Laboratoire d'Astrophysique de Marseille) UMR 7326, 13388, Marseille, France
[12] School of Earth and Space Exploration and Department of Physics, Arizona State University, Tempe, AZ 85287
[13] Université de Toulouse, UPS-OMP, Institut de Recherche en Astrophysique et Planétologie (IRAP), Toulouse, France
[14] CNRS, IRAP, 9 Av. colonel Roche, BP 44346, F-31028 Toulouse cedex 4, France
[15] University College London, Department of Physics and Astronomy, Gower Street, London WC1E 6BT, UK
[16] Institut d'Astrophysique de Paris, Sorbonne Universités, UPMC Univ. Paris 06, CNRS UMR 7095, 75014 Paris, France
[17] LERMA, CNRS, Observatoire de Paris, 61 avenue de l'Observatoire, Paris, France

Received January 19, 2018 / Accepted –

ABSTRACT

The Crab nebula is a supernova remnant exhibiting a highly polarized synchrotron radiation at radio and millimeter wavelengths. It is the brightest source in the microwave sky with an extension of few arcminutes and commonly used as standard candle for any experiment which aims at measuring the polarization of the sky. Though its spectral energy distribution has been well characterized in temperature, in polarization the amount of data is still mediocre. We report in this paper high resolution (18″ FWHM) observations of the Crab nebula in total intensity and linear polarization at 150 GHz with the *NIKA* camera. *NIKA*, operated at the IRAM 30 m telescope from 2012 to 2015, is a camera made of Lumped Element Kinetic Inductance Detectors (LEKIDs) observing the sky at 150 and 260 GHz. From these observations we are able to reconstruct the spatial distribution of the Crab nebula polarization degree and angle, which is found to be compatible with previous observations at lower and higher frequencies. Averaging across the source and using other existing data sets we find that the Crab nebula polarization angle is consistent with being constant over a wide range of frequencies with a value of $-88.1° \pm 0.3$ in Galactic coordinates. We also present the first estimation of the Crab nebula Spectral Energy Distribution polarized flux.
These measures underline the importance of a deep study of the polarization properties of the Crab nebula to be considered as absolute calibrator for both high resolution camera of ground based observatories and next generation of CMB experiments which aim at measuring the polarization of the sky.

Key words. Techniques: Crab nebula – Tau A – polarization – KIDs – individual: NIKA

1. Introduction

The Crab nebula (or Tau A) is a plerion-type supernova remnant emitting a highly polarized signal (Weiler & Panagia 1978; Michel et al. 1991). Referring to Hester (2008), from inside out the Crab consists of a pulsar, the synchrotron nebula, a bright expanding shell of thermal gas, and a larger very faint freely expanding supernova remnant.

Near the center of the nebula a shock is observed as formed by the jet thermalized and pulsar's ultra-relativistic wind which is confined by the thermal ejecta from the explosion (Weisskopf et al. 2000; Wiesemeyer et al. 2011). The synchrotron emission from the nebula is observed in the radio frequency domain as powered by the pulsar located at equatorial coordinates (J2000) $R.A. = 5^h34^m31.9383014^s$ and $Dec. = 22°0'52.17577''$ (Lobanov et al. 2011) through its jet.

⋆ Corresponding author: Alessia Ritacco, ritaccoa@iram.es

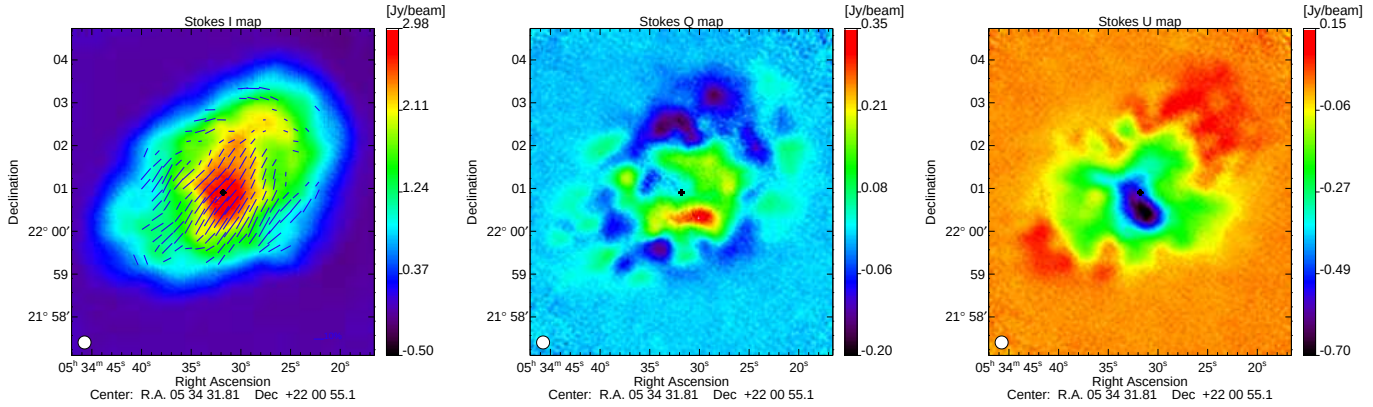

Fig. 1. From left to right: Crab nebula Stokes I, Q and, U maps shown here in Equatorial coordinates obtained at 150 GHz with the *NIKA* camera. Polarization vectors, indicating both the degree and the orientation, are over-plotted in white on the intensity map where the polarization intensity satisfies $I_{pol} > 3\sigma_{I_{pol}}$ and $I_{pol} > 0.1$ Jy. The *NIKA* FWHM is shown in the lower left. The black cross marks the pulsar position.

The polarization of the Crab nebula radio emission, discovered in 1957 independently by Mayer et al. (1957) and Kuz'min & Udal'Tsov (1959) has confirmed that the synchrotron emission as the underlying mechanism.

Today the Crab nebula is perhaps the most observed object in the sky beyond our own solar system and often used as calibrator by new instruments. It is also quite isolated with low background diffuse emission.

In particular it is the most intense polarized astrophysical object in the microwave sky at angular scales of few arcminutes and for this reason it is chosen not only for high resolution cameras but also for the calibration of CMB polarization experiments, which have beamwidths comparable to the extension of the source. Indeed, upcoming CMB experiments aiming at measuring the primordial $B-$modes require an accurate determination of the foreground emissions to the CMB signal and a high control of systematic effects. The Crab nebula has already used for polarization cross-check analysis in the frequency range from 30 to 353 GHz (Weiland et al. 2011; Planck Collaboration et al. 2016).

High angular resolution observations from the XPOL experiment (Thum et al. 2008) at the IRAM 30 m telescope have revealed the spatial distribution of the Crab Nebula in intensity and polarization at 90 GHz with an absolute accuracy of 0.5° in the polarization angle (Aumont et al. 2010). This observation has also showed that the polarization spatial distribution varies from the source peak to the edges of the source and evidences the need of an accurate study at high resolution in a large frequency range to be able to use this source as a calibrator for future polarization esperiments.

Such high resolution observations of the Crab nebula in polarization are crucial for future *NIKA2* polarization observations and could be very useful for the calibration of the next generation of polarization experiments.

Previous studies (Macías-Pérez et al. 2010) of the total Spectral Energy Distribution (SED) of the Crab nebula have shown a spectrum well described by a single synchrotron component at radio and mm wavelengths and predict negligible variations in polarization fraction and angle in the frequency range of interest for CMB studies.

Observations of the polarization of the Crab Nebula have been performed with the *NIKA* camera (Monfardini et al. 2010; Catalano et al. 2014; Monfardini et al. 2014) at the IRAM 30 m telescope during the observational campaign of February, 2015. A first overview of the *NIKA* Crab polarization observations, focusing on instrumental characterization of the polarization system, was given in Ritacco et al. (2016). In this paper we go a step further in the analysis by combining *NIKA* observations with published values at other frequencies to trace the polarized SED of the Crab nebula. We use polarization observations from the *WMAP* satellite at 23, 33, 41, 61 and 94 GHz (Weiland et al. 2011), from the *Planck* satellite at 30, 44, 70, 100, 143, 217, 353 GHz and from XPOL/30m at 90 GHz (Aumont et al. 2010).

The paper is organized as follows: in Sec. 2 the intensity and polarization maps obtained with the *NIKA* camera are presented together with the polarization degree and angle spatial distributions; Sec. 3 presents the reconstruction of the polarization properties of the Crab nebula in well defined regions; Sec. 4 presents the Crab nebula SED in temperature and polarization; in Sec. 5 we present our conclusions.

2. *NIKA* observations of the Crab Nebula

2.1. NIKA camera and polarization setup

NIKA is a dual band camera observing the sky in intensity and polarization at 150 and 260 GHz with 18 arcsec and 12 arcsec FWHM resolution, respectively. It has a Field-of-View (FoV) of 1.8′ at both wavelengths. It was operated at the IRAM 30 m telescope between 2012 and 2015. A detailed description of the *NIKA* camera can be found in Monfardini et al. (2010, 2011) and Catalano et al. (2014).

In addition to total power observations, *NIKA* was also a test bench for the polarization system of the final instrument *NIKA2* (Calvo et al. 2016; Catalano et al. 2016; Adam et al. 2017), which was installed at the telescope in October, 2015. The polarization setup of *NIKA* and *NIKA2* consists in a continuously rotating metal mesh half wave plate (HWP) followed by an analyzer, both at room temperature (for *NIKA*) and placed in front of the entrance window of the cryostat. The Lumped Elements Kinetic Inductance Detectors (LEKIDs) are not intrinsically sensitive to polarization. The HWP rotates at 2.98 Hz which modulates the polarization signal at 4×2.98 Hz. With a typical telescope scanning speed of 26.23 arcsec/s, this provides a quasi-simultaneous measure of Stokes parameters I, Q and U per beam and places the polarized power in the frequency domain far from the low frequency electronic noise and the atmospheric fluctuations. Ritacco, A. et al. (2017) gives more details on the *NIKA* polarization capabilities and describes the performance of the instrument at the telescope. In particular the sensi-

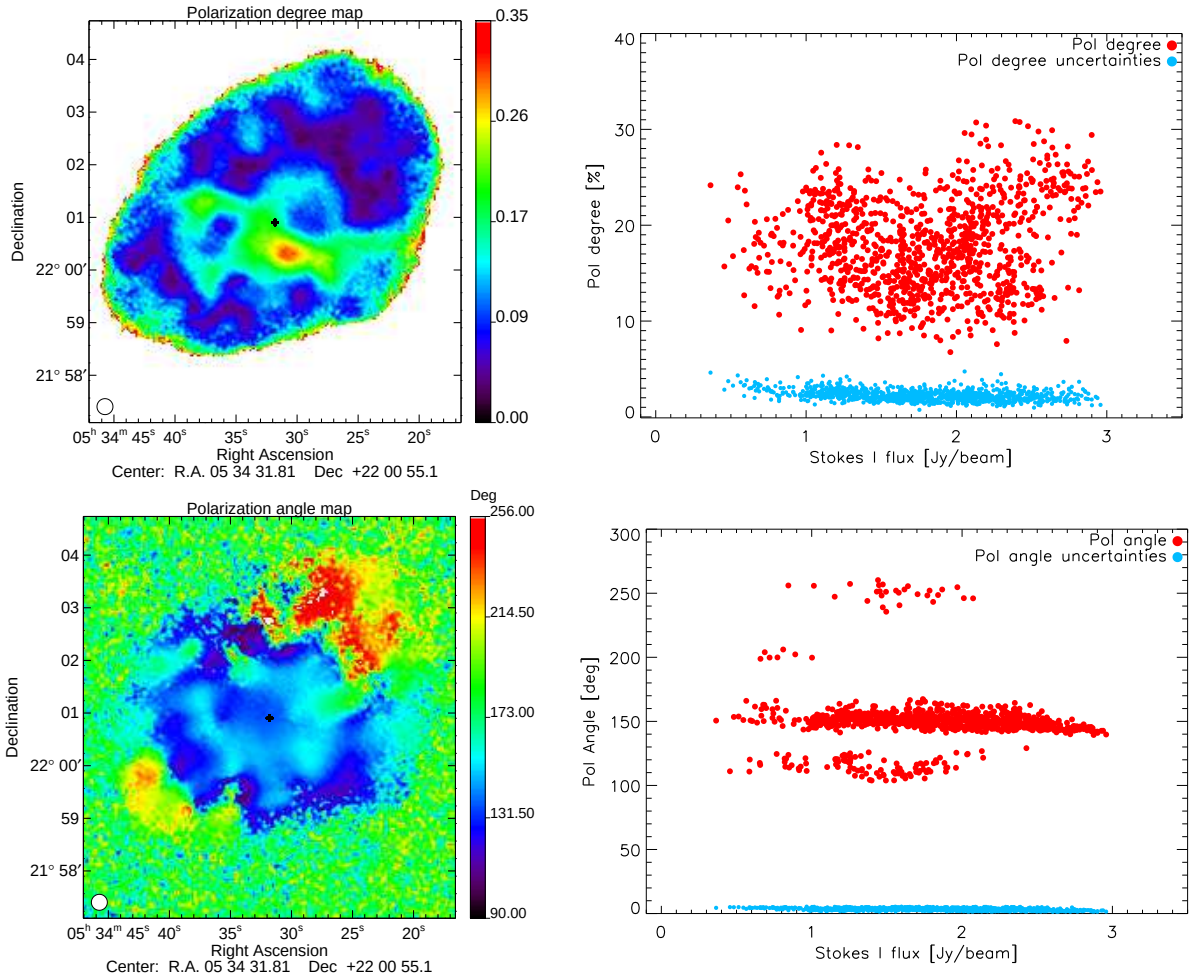

Fig. 2. *Top*: The left panel shows the polarization degree map p, uncorrected for noise bias, of the Crab nebula. The right panel shows the noise bias corrected p values as a function of total intensity map (Stokes I). The condition $I_{pol} > 5\sigma_{I_{pol}}$ is satisfied for those values. *Bottom*: on the left we present the polarization angle map ψ (Equatorial coordinates system) of the Crab nebula. On the right panel the distribution of ψ values is represented as a function of the total intensity in the case of very high S/N ratio where $I_{pol} > 5\sigma_{I_{pol}}$. The cyan dots represent the uncertainties calculated as the dispersion between different observational scans. The black cross marks the pulsar position on the maps.

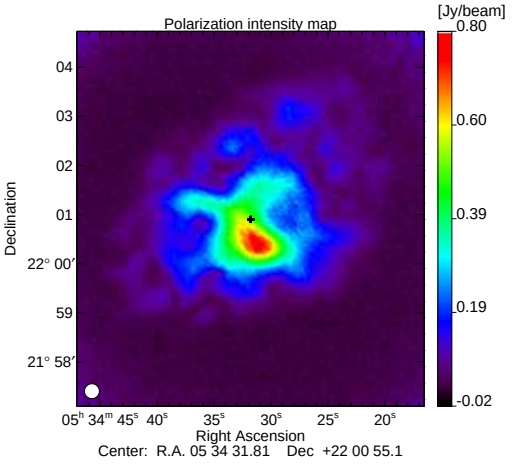

Fig. 3. *NIKA* polarized intensity map of the Crab nebula at 150 GHz. The map shows high polarized emission reaching a value of 0.8 Jy beam^{-1}. The telescope beam FWHM is shown in the lower left. The black cross marks the pulsar position.

tivity of the *NIKA* camera in polarization mode was estimated to be 50 mJy.$s^{1/2}$ at 150 GHz.

NIKA has provided the first polarization observations performed with Kinetic Inductance Detectors, confirming that KIDs are a suitable detector technology for the development of the next generation of polarization sensitive experiments.

2.2. NIKA observations

Crab nebula polarization observations with the *NIKA* camera were performed at the IRAM 30 m telescope in February, 2015. The average effective opacity at 150 GHz was $\tau = 0.2$. Fig. 1 shows the Stokes I, Q and U maps obtained by a co-addition of 14 maps of 8×6 arcminutes for a total observation time of $\sim$ 2.4 hours. The maps were performed in equatorial coordinates in four different scan directions: 0°, 90°, 120°, 150°. This allowed us to have the best coverage of the source.

To obtain the Stokes I, Q, and U Crab nebula maps in Equatorial coordinates, we have used a dedicated polarization data reduction pipeline (Ritacco, A. et al. 2017), which is an extension of the total intensity *NIKA* pipeline (Catalano et al. 2014; Adam et al. 2014). The main steps of the polarization pipeline are summarized below:

1. Subtraction of the HWP induced parasitic signal, which is modulated at harmonics of the HWP rotation frequency and

represents the most tedious noise contributing to the polarized signal.

2. Reconstruction of the Stokes I, Q and U time ordered information (TOI) from the raw modulated data. This is achieved using a demodulation procedure consisting in a lock-in around the fourth harmonic of the HWP rotation frequency, where the polarization signal is located.
3. Subtraction of the atmospheric emission in the demodulated TOIs using decorrelation algorithms. In polarization, the HWP modulation reduces significantly the atmospheric contamination and there is no need to further decorrelate the Q and U TOI's from residual atmosphere. By contrast, in intensity the atmospheric emission fully dominates the signal and to recover the large angular scales we use the 260 GHz band as an atmosphere dominated band like in Adam et al. (2014). This decorrelation impacts the reconstructed Stokes maps via a transfer function. We have estimated this function with simulated observations of diffuse emission that were passed through the data reduction pipeline, with the exact same scanning, sample flagging and data processing as real data. We found that the power spectrum of the output maps match that of the input one to better than 1% (resp. 5%) on scales smaller (resp. larger) than $\sim 1'$. The impact of the data processing is thus negligible compared to uncertainties on absolute calibration on small scales, and its moderate effect on large angular scales is further reduced with the subtraction of a zero level for the photometry (see below). In the following, we therefore neglect this transfer function.
4. Correction of the intensity-to-polarization-leakage-effect, which was identified in observations of unpolarized sources like the planet Uranus. For point sources the effect was about 3% peak-to-peak, while for extended sources like the Crab nebula it has been found to be the order of 0.5 % peak-to-peak. Ritacco, A. et al. (2017) describes the algorithm of leakage correction developed specifically for *NIKA* polarization observations. Applying this algorithm to Uranus observations the instrumental polarization is reduced to 0.6% of the total intensity I.
5. Projection of the demodulated and decorrelated Stokes I, Q, and U TOIs into Stokes I, Q and U equatorial coordinates maps.

2.3. Crab polarization properties

In this section we discuss the polarization properties of the source in terms of polarization degree p and angle ψ, which are defined through the Stokes parameters I, Q, and U as follows:

$$p = \frac{\sqrt{Q^2 + U^2}}{I}$$

and

$$\psi = \frac{1}{2} \arctan \frac{U}{Q}. \quad (1)$$

These definitions are not linear in I, Q and U and therefore, the observational uncertainties have to be carefully considered, *i.e.* p, ψ are noise biased. Simmons et al. (1980); Simmons & Stewart (1985); Montier et al. (2015) proposed analytical solutions to correct for this bias. For intermediate and high S/N ratio the polarization degree and its uncertainty read:

$$\begin{aligned} p &= \frac{\sqrt{Q^2 + U^2 - \sigma_Q^2 - \sigma_U^2}}{I}, \\ \sigma_p &= \frac{\sqrt{Q^2\sigma_Q^2 + U^2\sigma_U^2 + p^4 I^2 \sigma_I^2}}{pI^2}. \end{aligned} \quad (2)$$

Furthermore, the polarization angle in a high S/N regime can be approximated by Eq. 1 with the uncertainty

$$\sigma_\psi = \frac{\sqrt{Q^2\sigma_Q^2 + U^2\sigma_U^2}}{2(pI)^2}. \quad (3)$$

The angular distribution map of the polarization degree p of the Crab nebula without noise bias correction is presented on the top left panel of Fig. 2. **Tab. 1 presents the total flux I, Q, and U, the polarization intensity, degree p, and angle ψ computed at the pulsar position, highlighted by a black cross on maps, and at the Stokes I peak position. The values have been estimated integrating the total flux in a beam-like the map-pixel size, *i.e.* 2 arcsec, and in a beam-like *NIKA* at 2mm of 18.2″. Clearly the total flux in I, Q, and U is different but the polarization degree and angle are consistent between each other.**

The polarization degree p reaches a value of 20.9 ±0.8 % at the peak of the total intensity, which is consistent with what observed on the top right panel of Fig. 2, where the variation of p as a function of the Stokes I is shown. Here the p values have been noise bias corrected and satisfy the condition $I_{pol} = \sqrt{Q^2 + U^2} > 5\,\sigma_{I_{pol}}$. The distribution of the polarization degree appears highly dispersed around a mean value of 20%. The compatibility between the p value computed at the Stokes I peak position and the above mentioned plot is expected because we use a very high S/N ratio threshold of 5 $\sigma_{I_{pol}}$, which restricts the measurement to a small region around the peak of the source. In addition, the p value found is also consistent within the error bars with POLKA experiment measurement (Wiesemeyer et al. 2014) (cf. Table 2).

The polarization degree decreases towards the edges of the source. Furthermore, the high polarization degree observed at the extremities of the source is misleading and caused by the very low S/N ratio of the Stokes I map observed in these regions. The variation of p highlights the interest of high resolution polarization observations of the Crab nebula.

The bottom left panel of Fig. 2 shows the spatial distribution of polarization angle ψ. We observe a relatively constant polarization angle of about 150 ° represented here in equatorial coordinates, except for the northern region where the averaged angle is around 220°, and some inner regions with lower polarization angle. These values are confirmed by the bottom right panel that shows the polarization angle distribution as a function of total intensity satisfying the condition $I_{pol} > 5\sigma_{I_{pol}}$.

The sudden change of polarization angle on the northern region was already observed by the XPOL experiment at 90 GHz (Aumont et al. 2010). This together with the variation of the polarization fraction discussed above confirms the need of high angular resolution observations at low and high frequencies for a good understanding of the Crab polarized emission properties. High resolution observations give the possibility to estimate the polarization properties at different scales and compare with low resolution experiments, like CMB experiments.

We present in Fig. 3 the 150 GHz Crab polarization intensity map I_{pol} uncorrected for noise bias. We observe a peak at 0.8 Jy beam^{-1} and the polarization decreases towards the edges of the nebula.

	I [Jy]	Q [Jy]	U [Jy]	I_{pol} [Jy]	p [%]	ψ [°]
A pixel beam size						
Peak	0.219 ± 0.001	0.0053 ± 0.0047	-0.045 ± 0.001	0.045 ± 0.001	20.7 ± 0.7	138.3 (-80.7) ± 2.3 ± 1.8
Pulsar	0.212 ± 0.001	0.0037 ± 0.0027	-0.039 ± 0.002	0.039 ± 0.002	18.6 ± 1.2	137.7 (-80.1) ± 1.3 ± 1.8
***NIKA* beam size**						
Peak	8.28 ± 0.12	0.31 ± 0.06	-1.70 ± 0.05	1.73 ± 0.05	20.9 ± 0.8	140.20 (-82.6) ± 0.04 ± 1.8
Pulsar	8.39 ± 0.07	0.19 ± 0.06	-1.52 ± 0.06	1.52 ± 0.06	18.1 ± 0.8	138.51 (-80.9)± 0.09 ± 1.8

Table 1. Flux densities in total power, polarization, degree and angle of the polarization estimated at the peak position of the Stokes I map. The position of the pulsar, represented on the maps by a black cross, refers to Lobanov et al. (2011). The position of the peak of the total intensity has coordinates equatorial coordinates (J2000) $R.A. = 5^h34^m32.380422^s$ and $Dec. = 22°0'44.098276''$. The polarization angle is given in Equatorial coordinates and in Galactic coordinates within parenthesis. A systematic angle uncertainty of 1.8° must be considered. A total calibration error of 10 % must be accounted for and propagated to the polarization estimates.

	I [Jy]	p [%]	ψ [°]
		Pulsar	
POLKA	1.63	25.3 ± 3.0	145.1 ± 3.3
XPOL		13.9 ± 0.6	158.1 ± 0.5
SCUPOL		14.3 ± 1.8	140.0 ± 2.8
		Peak	
POLKA	1.72	25.0 ± 3.1	151.7 ± 3.5
XPOL		25	149.0 ± 1.4
SCUPOL		18.7 ± 1.5	146.1 ± 2.1

Table 2. Values estimated by POLKA (870 μm), XPOL (3 mm), SCUPOL (850 μm) reported in Wiesemeyer et al. (2014) at the pulsar and peak position, respectively.

3. Total intensity and polarization fluxes

We compute the total flux across the Crab nebula, which has an extent of about 5′x7′ as shown in Fig. 1. We use standard aperture photometry techniques to calculate the flux as shown in Fig. 4. We use as center position the center of the map. A zero level in the map, calculated as the mean of the signal measured on an external annular ring region (see bottom panel of Fig. 4) of radius $4' < R < 4.5'$, has been subtracted from the map. The total signal estimated is 204.4±7.9±10.2 Jy. The first uncertainty term accounts for statistical uncertainties computed from fluctuations of the signal at large radii. We use Uranus for absolute point source flux calibration. The flux of the planet is estimated from a frequency dependent model of the planet brightness temperature as described in Moreno (2010). This model is integrated over the *NIKA* bandpasses for each channel, and it is assumed to be accurate at the 5% level. The final absolute calibration factor is obtained by fitting the amplitude of a Gaussian function of fixed angular size on the reconstructed maps of Uranus, which represents the main beam. For the polarization observational campaign of February 2015 this uncertainty is estimated to be 5% for the *NIKA* 2.05 mm channel (150 GHz) (Ritacco, A. et al. 2017). Nevertheless, as described in Adam et al. (2014); Catalano et al. (2014), by integrating the Uranus flux up to 100 arcsec, we observe that the total solid angle covered by the beam is larger than the Gaussian best-fit of the main beam by a factor of 28%. As consequence we account for this factor in the estimation of the fluxes. Moreover, Adam et al. (2014) estimated the uncertainty on the solid angle of the main beam to be 4%. Finally, the overall calibration error is estimated to be about 10%, by considering also the uncertainties on the side lobes.

The polarization efficiency factor estimated across the *NIKA* 2.05 mm spectral band and reported in Ritacco, A. et al. (2017) is $\rho_{pol} = 0.9941 \pm 0.0002$. This very small efficiency lost of 0.6 % has a very small impact on the estimation of the polarization fluxes and the calibration error itself.

In order to compare our results with low angular resolution CMB experiments, we present in Tab. 3 the polarization degree p and angle ψ integrated values obtained in well defined regions: 5′, 7′ FWHM from the center of the maps, at the pulsar position and Stokes I peak position.

The polarization angles are here presented in Equatorial coordinates and Galactic coordinates, within parenthesis, to ease the comparison with the *Planck* (Planck Collaboration et al. 2016) and *WMAP* CMB experiments (Weiland et al. 2011). As discussed in Ritacco, A. et al. (2017) a 1.8° uncertainty must be considered because the mechanical motor, in which the HWP is mounted, completes 100 steps per tour of the HWP. Therefore, it is the precision associated to the determination of the HWP zero, corresponding to its optical axis in the cabin reference frame.

Notice that the *Planck* satellite FWHMs are: 33′, 24′, 14′, 10′, 7.1′, 5.5′, 5′ arcminutes at 30, 44, 70, 100, 143, 217, 353 GHz, respectively. *WMAP* satellite has FWHMs: 0.93°, 0.68°, 0.53°, 0.35°, <0.23° at 22 GHz, 30 GHz, 40 GHz, 60 GHz, 90 GHz respectively.

As stated in 2.3, we use simple Gaussian estimators in this work that are unbiased only at high S/N ratio. This adds an additional uncertainty on the determination of the degree of polarization p and on the angle ψ when the SNR is not larger than $\sim 3\sigma$. While we can delimit regions of the map as a function of their SNR to give reliable results per pixel, the determination of average quantities over the entire map is more delicate. Intensity does not suffer from this limitation, so the average flux of the source can safely be integrated over all pixels. **Taking the entire map and averaging it over Gaussian beams of 5′ and 7′ FWHM, we find $\psi = -83.3 \pm 1.9° \pm 1.8°$ and $\psi = -81.7 \pm 3.7° \pm 1.8°$ respectively, while we find $-87.6 \pm 0.6° \pm 1.8°$ if we consider only pixels with a I_{pol} SNR larger than 3 in both regions. The angle averaged in the Gaussian beams are more affected by the noise on the maps but still consistent with the case of high S/N. In terms of polarization degree, we find $p = 6.7 \pm 0.4\%$ and $p = 6.9 \pm 0.2$ if we take all the pixels to average Q and U over our fiducial beams of 5′ and 7′, respectively. The statistical uncertainty accounts for montecarlo simulation of the noise in Q and U, the angle estimation difference between two sets of jack-knife maps, 7 maps each. Morevover for the polarization angle we account for the uncertainty due to leakage effect subtraction of 0.5°, which has been found comparing the maps before and after leakage correction.** Fig. 5 shows the polarization fraction (top) and polarization angle (bottom) of the Crab nebula as a function of the frequency as measured by five different instruments: *Planck* (Planck Collaboration et al.

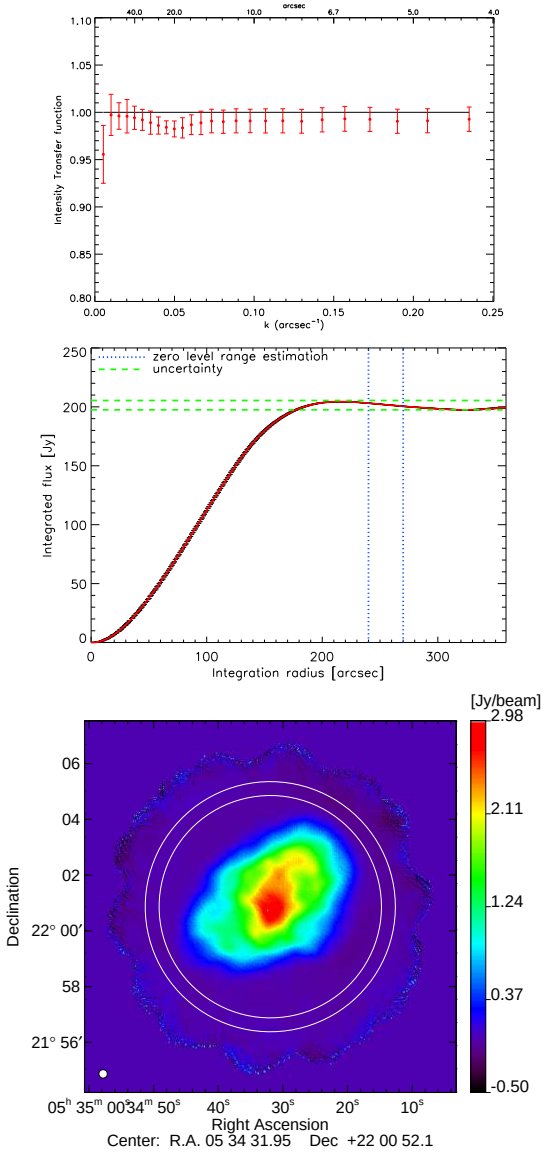

Fig. 4. Top: Transfer function of the intensity data processing. Middle: Cumulative flux of the Crab nebula (top) obtained at 150 GHz over 4′ from the center obtained by aperture photometry. The flux has been corrected by a zero level in the map, which corresponds to the mean of the signal calculated in an annular ring as indicated by the white circles on the map (bottom) and by the blue dotted lines on the top. The green dotted line represents the uncertainties measured at large radii.

2016), *WMAP* (Weiland et al. 2011), XPOL (Aumont et al. 2010) and *NIKA* (this paper).

The solid line in both figures represents the weighted-average found using all the observations shown and the dashed lines represent the uncertainties estimated on the weighted-average. Considering only low frequency data (<200 GHz) and excluding the XPOL data (see below) we find that the degree of polarization of the Crab nebula at arcmin scales is 7.1±0.1 %. In terms of degree of polarization most data sets are consistent at the 2σ level with the weighted-average value. For XPOL the discrepancy can probably be explained by the lower sensitivity of the single channel XPOL experiment to the lower than average polarization of the outer parts of the nebula.

In the case of *Planck* the observed discrepancy at high frequency could be due to an evolution of the Crab nebula polarization properties with frequency, but this hypothesis is disfavored by the polarization angle measurements that seem to be consistent with the mean value across all frequencies.

The weighted-average of the polarization angle of the Crab nebula at ≥ 5′ scales is therefore estimated considering all available observations, is -88.1° ± 0.3. All the observations shown on the bottom panel of Fig. 1 agree within 1σ with this value except for the *Planck* value at 30 GHz, which is slightly high.

Tab. 2 reports the measurement of the polarization properties, degree and angle, performed by the POLKA, XPOL and SCUPOL experiments Wiesemeyer et al. (2014). These three experiments observing at wavelengths of 870 μm, 3 mm and 850 μm, respectively, show a significant discrepancy in terms of polarization angle estimated at the pulsar position. Though POLKA and SCUPOL agree at 1σ level, XPOL show a much higher angle. At the position of the peak of the total intensity the three experiments are consistent between each other. Tab. 1 shows the values estimated with the *NIKA* camera on the 2 mm maps. We present the flux densities of Stokes I, Q, and U, the polarization intensity flux $I_{\rm pol}$, the polarization degree p and the polarization angle ψ for the position mentionned above computed in a pizel beam size, *i.e.* 2″, and *NIKA* beam size, *i.e.* 18.2″. In the first case we notice that the estimated $Q \simeq \sigma_Q$, the total polarization flux is entirely located in U. The low S/N in Q contributes to the increase of the uncertainty σ_ψ. Generally, the values estimated with *NIKA* are consistent within 3σ level with POLKA and SCUPOL experiments, but they disagree the XPOL values, which show higher values in both positions. We also notice that the total flux measured varies significantly if we integrate in 2″ or 18″.

4. Crab Spectral Energy Distribution in intensity and polarization

4.1. Intensity

The total intensity emission of the Crab nebula at radio and millimeter wavelengths (from 1 to 500 GHz) is mainly due to synchrotron emission and can be well described by a single power law of the form:

$$I_\nu = A(\nu/1\mathbf{GHz})^\beta \qquad (4)$$

with spectral index β = -0.296±0.06 (Baars et al. 1977; Macías-Pérez et al. 2010). Further, the Crab nebula is fading with time at a rate of α = 0.167±0.015 % yr^{-1} (Aller & Reynolds 1985). These results suggest a low frequency emission produced by particles accelerated by the same magnetic field. Macías-Pérez et al. (2010) have shown also that there is no evidence for an extra synchrotron component and for a component of thermal dust emission at these frequencies. The direction of the polarization is therefore expected to be constant across the frequency range 30-300 GHz while the polarization degree may vary.

We show in Fig. 6 the flux of the Crab nebula as a function of frequency. The fluxes in the radio domain were taken from Dmitrenko et al. (1970) and Vinogradova et al. (1971). We also show microwave and mm wavelengths fluxes from *Archeops* (Macías-Pérez et al. 2007), *Planck* (Planck Collaboration et al. 2016), WMAP (Weiland et al. 2011), XPOL/30m (Aumont et al. 2010), MAMBO/30m (Bandiera et al. 2002) and GISMO/30m (Arendt et al. 2011). The measured *NIKA* total intensity flux at 150 GHz is shown in red.

	I [Jy]	Q [Jy]	U [Jy]	I_{pol} [Jy]	p [%]	ψ [°]	$I_{pol} > 3\sigma_{I_{pol}}$
7′ FWHM centered	216.8 ± 5.9	2.3±0.8	-14.9 ±0.5	15.0 ±0.3	6.9±0.2	139.3(-81.7)±3.2±1.8*	145.2(-87.6)±0.1±1.8*
5′ FWHM centered	218.3 ± 5.5	3.0 ±0.5	-14.2±0.6	14.5±0.5	6.7±0.4	140.0(-83.3)±1.4±1.8*	145.2(-87.6)±0.1±1.8*

Table 3. *A systematic angle uncertainty of 1.8° must be considered in the polarization angle error budget. Total flux I, Q, and U, polarized intensity flux I_{pol}, polarization degree p, and angle ψ are here presented. The values have been calculated within 7′ and 5′ radius from the center of the map. The polarization angle has been also calculated where $I_{pol} > 3\sigma_{I_{pol}}$ to avoid the contribution of pixels biased by the noise. The polarization angle is here given in Equatorial coordinates and Galactic coordinates within parenthesis. A total calibration error of 10 % must be accounted for and propagated to the polarization estimates.

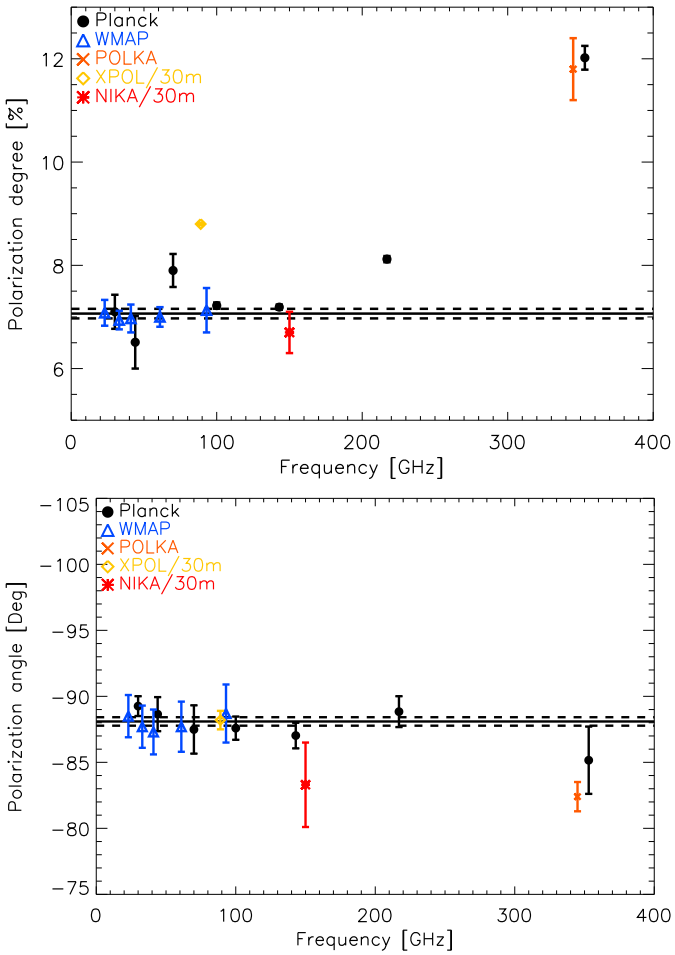

Fig. 5. *Top*: polarization degree as a function of frequency as measured by *Planck* (black dots), WMAP (blue triangles), XPOL (green diamond) and *NIKA* (red crosses). The *NIKA* value has been estimated by integrating in a radius of 5′ as given by XPOL (Aumont et al. 2010). The solid line represents the weighted-averaged degree of polarization accounting for low frequency values (<200 GHz) and excluding XPOL. Dashed lines are the uncertainties. *Bottom*: polarization angles in Galactic coordinates for the same five experiments given above. The solid line represents the weighted-averaged polarization angles.

Accounting for the break shown by *Planck* satellite data we assume a simple two-power-law model[1]:

$$I_\nu = \begin{cases} A_L(\nu/1GHz)^{\beta_L} & \nu < 90\ \mathbf{GHz} \\ A_H(\nu/1GHz)^{\beta_H} & \nu \geq 90\ \mathbf{GHz} \end{cases} \quad (5)$$

By χ^2-minimization we obtain the fit shown in cyan in Fig. 6, where the cut-off frequency is 90 GHz and the knee frequencies are: 8 GHz and 100 GHz. The best-fit parameters obtained are:

$$A_L = 507.7 \pm 0.1; \quad \beta_L = -0.3187 \pm 0.0001$$
$$A_H = 216.4 \pm 0.3; \quad \beta_H = -0.7525 \pm 0.0003$$

[1] A detailed physical description of the SED of the Crab nebula is out of the scope of this paper.

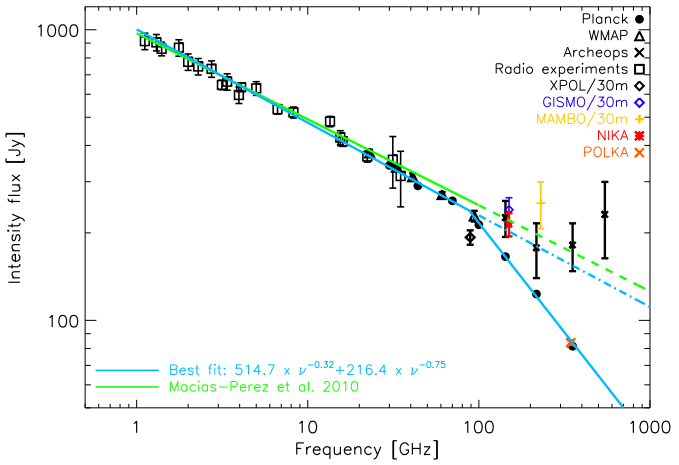

Fig. 6. Crab nebula total intensity SED as obtained from *Planck* (Planck Collaboration et al. 2016), *WMAP* (Weiland et al. 2011), Archeops (Macías-Pérez et al. 2007), radio experiments (Dmitrenko et al. 1970; Vinogradova et al. 1971), XPOL/30m (Aumont et al. 2010), *NIKA*30m (this paper), MAMBO/30m (Bandiera et al. 2002) and GISMO/30m (Arendt et al. 2011) data. The green line shows the model derived by a previous analysis discussed in (Macías-Pérez et al. 2010). The best-fit obtained by the analysis in this paper is shown in cyan line. Both, the best-fit models and the data account for the Crab nebula fading with the time.

We notice that *NIKA* data is consistent with this model at the 2σ level. More data at mm wavelengths are needed to better understand the observed break of the SED around 90 GHz.

For illustration we also show in green line the best-fit model as result of a previous study Macías-Pérez et al. (2010). Notice that in the plot both the best-fit model and the data represented accounts for the fading of the source. The estimated spectral index β_L is slightly different if we compare with the previous estimation provided by Macías-Pérez et al. (2010). This mainly concerns the addition of recently published results by *Planck* (Planck Collaboration et al. 2016) and WMAP (Weiland et al. 2011). *NIKA* camera agrees at 1 σ level with both models. As already discussed above XPOL/30m total power emission is low with respect to expectations from both power law models.

The *Planck* data at 100, 143, 217 and 353 GHz appears to be consistent with a much steeper SED with respect to the lower frequency data. This trend suggests an extra emission component due to a different population of relativistic electrons (Ginzburg & Syrovatskii 1965; Gomez et al. 2012) which to date has not been identified with other experiments.

By contrast *Archeops*, MAMBO/30m, GISMO/30m and *NIKA*/30m do not seem to support such a low frequency break in the Crab nebula SED. In addition, Macías-Pérez et al. (2010) discusses this possibility but only for higher frequency above 1000 GHz, where few observations evidences a break in the power law. **This section figures out a clear inconsistency of recent *Planck* data with low and high frequency data. In particular they show the evidence of a break in the power law around 90-100 GHz suggesting a different origin of the emission and/or the presence of a second population of electrons. This should be investigate more with high angular resolution observations which will permit to probe the small and large angular scales.**

4.2. Polarization

Though the total power emission of the Crab nebula has been monitored over decades across a large range of frequencies, the amount of polarization data is very small. Recent results provided by *Planck* (Planck Collaboration et al. 2016), *WMAP* (Weiland et al. 2011) and XPOL (Aumont et al. 2010) together with *NIKA* allow us to trace the spectral energy distribution of the polarized emission as shown in Fig. 7. Notice that the uncertainty for the *NIKA* value has been estimated propagating the absolute calibration error.

***Planck* data show an oscillating behaviour which is in contrast with what has been previously observed by *WMAP* satellite. The comparison between the two satellites at lower frequencies teases the question about the photometry of the *Planck* LFI for different frequencies. Whereas the *Planck* data at 100 GHz shows again a break of the power law, the point at 353 GHz follows a completely different trend. By contrast the *WMAP* data, although only at low frequencies, show a self-consistent power law model. Even if the comparison between the *WMAP* and *Planck* satellites is out the scope of this paper, we have decided to account for the two different trends shown by their results. Considering Eq. 4.1 as single power law like model for synchtron emission we use separately the *Planck* and *WMAP* data.** In Fig. 7 the two best-fit models are shown in blanck and blue for *Planck* and *WMAP* data, respectively.

Accounting for fading the best-fit parameters $A_w, \beta_w, A_p, \beta_p$ for *WMAP* and *Planck* fits, respectively are:

$$A_w = 78.98 \pm 7.82; \qquad \beta_w = -0.35 \pm 0.03$$
$$A_p = 116.46 \pm 6.52; \quad \beta_p = -0.45 \pm 0.01$$

XPOL and *NIKA* agree both power laws within 1σ error bar. In this case the XPOL data are not affected by the Stokes *I* map quality as in the case of the polarization degree measurement. If the *WMAP* best-fit model is in agreement with *Planck* observations at 30, 100 and 353 GHz, the *Planck* best-fit model seems to overestimate the polarization flux at low frequency. In contrast to the intensity data, here a 100 GHz break is less conspicuous. We find no clear hint of a break in the polarization SED at frequencies above 90 GHz, hence putting pressure on the hypothesis of multiple electron populations to explain the SED break in total power emission.

We have also estimated the spectral index of the Crab nebula polarization emission at high frequency using the map obtained by SCUPOL (Matthews et al. 2009) at 352 GHz (850 μm) and the *NIKA* map. Considering only the region observed by SCUPOL we obtain:

$$\beta_p = -0.33 \pm 0.01. \qquad (6)$$

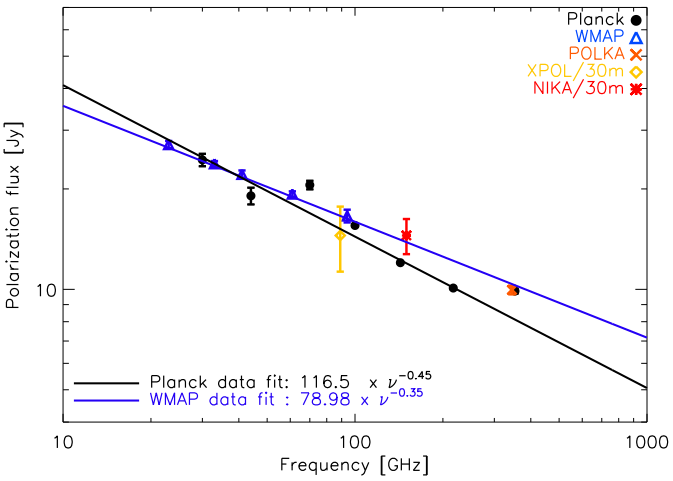

Fig. 7. Crab nebula polarization flux SED as obtained from the *Planck* (Planck Collaboration et al. 2016), *WMAP* (Weiland et al. 2011) and *NIKA* (this paper) data. The two best-fit models presented have been estimated using only WMAP data (blue line) or *Planck* data only (black line).

This result is in good agreement with the *WMAP* best-fit model spectral index.

From this analysis we noticed that the small amount of information at millimeter wavelengths in polarization emission is not conclusive but rather open several questions about the morphology of the polarized emission of the Crab nebula above 200 GHz. In the context of the *NIKA*2 instrument we aim to further investigate this aspect thanks to its polarized channel at 260 GHz.

5. Conclusions

The Crab nebula is considered as a celestial standard calibrator for CMB experiments in terms of polarization degree and angle. An absolute calibration is particularly important for the measurement of the CMB polarization B-modes, which are a window towards the physics of the early Universe.

We have reported in this paper first high angular resolution polarization observations of the Crab nebula at 150 GHz with the *NIKA* camera. These observations have allowed us to accurately map the spatial distribution of the polarization fraction and angle. Using all available polarization data to date we conclude that the polarization angle of the Crab nebula is consistent with being constant with frequency, from 23 GHz to 217 GHz, at arcmin scales with a value of -88.1° ±0.3 in Galactic coordinates. In addition, there is a strong case for a constant polarization degree below 200 GHz consistent with a value of $p = 7.1 \pm 0.1\%$. Above this frequency, *Planck* results are not consistent to each other.

Moreover, we have characterized the intensity and polarization SED of the Crab nebula. In intensity, recent *Planck* data show a break in the SED that could be explained by the existence of different populations of relativistic electrons. However, they are inconsistent with other data. In polarization, we find that the data are overall consistent with a single power law spectrum as expected from synchrotron emission. However, we find some discrepancies between data sets, which will require further mm measurements at high resolution for a better understanding of the physics at play. Among future polarization experiments, *NIKA2* (Calvo et al. 2016), will provide high sensitive polariza-

tion observations of the Crab nebula adding a 260 GHz map at 11″ resolution.

References

Adam, R., Adane, A., Ade, P. A. R., et al. 2017, ArXiv e-prints arXiv:1707.00908
Adam, R., Comis, B., Macías-Pérez, J. F., et al. 2014, A&A, 569, A66
Aller, H. & Reynolds, S. 1985, The Astrophysical Journal, 293, L73
Arendt, R. G., George, J. V., Staguhn, J. G., et al. 2011, ApJ, 734, 54
Aumont, J., Conversi, L., Thum, C., et al. 2010, A&A, 514, A70
Baars, J., Genzel, R., Pauliny-Toth, I., & Witzel, A. 1977, Astronomy and Astrophysics, 61, 99
Bandiera, R., Neri, R., & Cesaroni, R. 2002, A&A, 386, 1044
Calvo, M., Benoît, A., Catalano, A., et al. 2016, Journal of Low Temperature Physics, 184, 816
Catalano, A., Adam, R., Ade, P., et al. 2016, arXiv preprint arXiv:1605.08628
Catalano, A., Calvo, M., Ponthieu, N., et al. 2014, A&A, 569, A9
Dmitrenko, D., Tseitlin, N., Vinogradova, L., & Giterman, K. F. 1970, Radiophysics and Quantum Electronics, 13, 649
Ginzburg, V. L. & Syrovatskii, S. I. 1965, ARA&A, 3, 297
Gomez, H. L., Krause, O., Barlow, M. J., et al. 2012, ApJ, 760, 96
Hester, J. J. 2008, ARA&A, 46, 127
Kaufman, J., Leon, D., & Keating, B. 2016, International Journal of Modern Physics D, 25, 1640008
Kuz'min, A. D. & Udal'Tsov, V. A. 1959, Soviet Ast., 3, 39
Lobanov, A. P., Horns, D., & Muxlow, T. W. B. 2011, A&A, 533, A10
Macías-Pérez, J., Lagache, G., Maffei, B., et al. 2007, Astronomy & Astrophysics, 467, 1313
Macías-Pérez, J. F., Mayet, F., Aumont, J., & Désert, F.-X. 2010, ApJ, 711, 417
Matthews, B. C., McPhee, C. A., Fissel, L. M., & Curran, R. L. 2009, ApJS, 182, 143
Mayer, C. H., McCullough, T. P., & Sloanaker, R. M. 1957, ApJ, 126, 468
Michel, F. C., Scowen, P. A., Dufour, R. J., & Hester, J. J. 1991, ApJ, 368, 463
Monfardini, A., Adam, R., Adane, A., et al. 2014, Journal of Low Temperature Physics, 176, 787
Monfardini, A., Benoit, A., Bideaud, A., et al. 2011, ApJS, 194, 24
Monfardini, A., Swenson, L. J., Bideaud, A., et al. 2010, A&A, 521, A29
Montier, L., Plaszczynski, S., Levrier, F., et al. 2015, A&A, 574, A136
Moreno, R. 2010, Neptune and Uranus planetary brightness temperature tabulation, Tech. rep., ESA Herschel Science Center, available from ftp://ftp.sciops.esa.int/pub/hsc-calibration/PlanetaryModels/ESA2
Planck Collaboration, Ade, P. A. R., Aghanim, N., et al. 2016, A&A, 594, A26
Ritacco, A., Adam, R., Adane, A., et al. 2016, Journal of Low Temperature Physics, 184, 724
Ritacco, A., Ponthieu, N., Catalano, A., et al. 2017, A&A, 599, A34
Simmons, J. F. L., Aspin, C., & Brown, J. C. 1980, A&A, 91, 97
Simmons, J. F. L. & Stewart, B. G. 1985, A&A, 142, 100
Thum, C., Wiesemeyer, H., Paubert, G., Navarro, S., & Morris, D. 2008, PASP, 120, 777
Vinogradova, L. V., Dmitrenko, D. A., & Tsejtlin, N. M. 1971, Izvestiia Vysshaia Uchebn. Zaved., Radiofizika, 14, 157
Weiland, J. L., Odegard, N., Hill, R. S., et al. 2011, ApJS, 192, 19
Weiler, K. W. & Panagia, N. 1978, A&A, 70, 419
Weisskopf, M. C., Hester, J. J., Tennant, A. F., et al. 2000, ApJ, 536, L81
Wiesemeyer, H., Hezareh, T., Kreysa, E., et al. 2014, PASP, 126, 1027
Wiesemeyer, H., Thum, C., Morris, D., Aumont, J., & Rosset, C. 2011, A&A, 528, A11

Acknowledgements. We would like to thank the IRAM staff for their support during the *NIKA* campaigns. The NIKA dilution cryostat has been designed and built at the Institut Néel. In particular, we acknowledge the crucial contribution of the Cryogenics Group, and in particular Gregory Garde, Henri Rodenas, Jean Paul Leggeri, Philippe Camus. This work has been partially funded by the Foundation Nanoscience Grenoble, the LabEx FOCUS ANR-11-LABX-0013 and the ANR under the contracts "MKIDS", "NIKA" and ANR-15-CE31-0017. This work has benefited from the support of the European Research Council Advanced Grant ORISTARS under the European Union's Seventh Framework Programme (Grant Agreement no. 291294). We acknowledge fundings from the ENIGMASS French LabEx (R. A. and F. R.), the CNES post-doctoral fellowship program (R. A.), the CNES doctoral fellowship program (A. R.) and the FOCUS French LabEx doctoral fellowship program (A. R.).